Predicting Activity Using the Electrostatic Complementarity™ of Protein-ligand Complexes

Suneel Kumar, Tim Cheeseright, Matthias R. Bauer, Mark D. Mackey

Cresset, Cambridgeshire, UK suneel@cresset-group.com cresset-group.com

Abstract

Typical electrostatic interactions between small molecules and their respective receptors include hydrogen bonding, ionic, cation-π, π-π, lone-pair sigma-hole (halogen bonding), and orthogonal multipolar interactions (fluorine bonding). These interactions are essential for molecular recognition and are also key contributors to the binding free energy ΔG (enthalpic term) of protein-ligand complexes. Assessing the electrostatic match between ligands and binding pockets provides therefore important insights into why ligands bind and what can be changed to improve binding. We present the theoretical background of the Electrostatic Complementarity™ (EC) component of our structure-based design application, Flare™,[1] along with several examples showing the practical application of the scores to the prediction of activity and of the visualization to ligand design.

Method

The base of electrostatic potential calculations is the polarizable XED force field,[2,3] which enables description of atomic anisotropic charge distribution (usually only possible with *ab initio* methods). As described,[4] the electrostatic potential can be calculated:

$$(1)\quad V_c = \sum_{1}^{i} \frac{1}{4\pi\varepsilon_0} \frac{q_p q_i}{r_{i,p}} \frac{332.17}{D(r)}$$

The protein-ligand EC is calculated from comparison of protein and ligand electrostatic potentials (ESP) values at all vertex points of a generated ligand or protein solvent accessible surface (SAS). One option to assess EC is to employ an inverse Pearson R correlation test on the raw protein and ligand electrostatic potentials.

$$(2)\quad EC_R = r_{ESP_L,ESP_P} = -1 \times \frac{1}{n-1} \sum_{i=1}^{n} \left(\frac{ESP_{L_i} - \overline{ESP_L}}{s_{ESP_L}} \right) \times \left(\frac{ESP_{P_i} - \overline{ESP_P}}{s_{ESP_P}} \right)$$

We use an additional score that approximately corrects for some desolvation effects by capping the ligand and protein ESP values to the maximum ESP values observed for water. This score also allows local visualization of EC on a protein or ligand solvent-accessible surface.

$$(3)\quad EC = \iint_S \left(1 - \frac{ESP_L + ESP_P}{max(ESP_L, ESP_P, k)} \right) dS$$

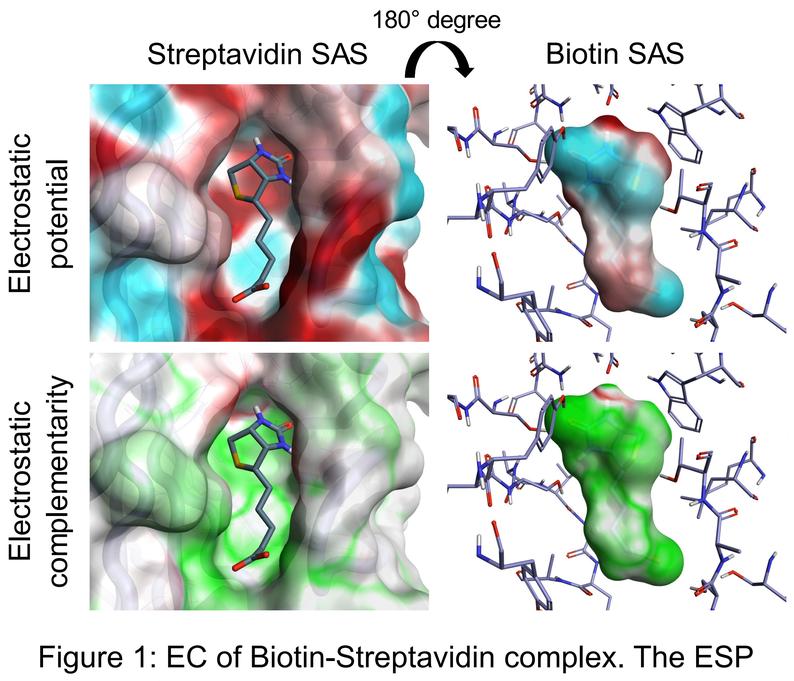

Figure 1: EC of Biotin-Streptavidin complex. The ESP of protein and ligand (blue = negative and red = positive electrostatic potential) and the protein-ligand EC (green = complementary, red = electrostatic clash) are shown.

Caveats

EC does not compute ΔG and can not predict changes in activity due to conformational effects, hydrophobic space filling, and solvent effects.

Results

mGLU5

Starting from a fragment hit against a thermostabilized metabotropic glutamate mGLU5 GPCR, Christopher *et al*. recently developed negative allosteric modulator lead compounds using X-ray crystallography and structure-based design.[6] X-ray structures of the most active compounds in complex with mGLU5 served as starting points for model building (5CGC and 5CGD). The published SAR, comprising 22 compounds, contained several changes in bioactivity that appear to be mainly driven by changes in ligand electrostatics.

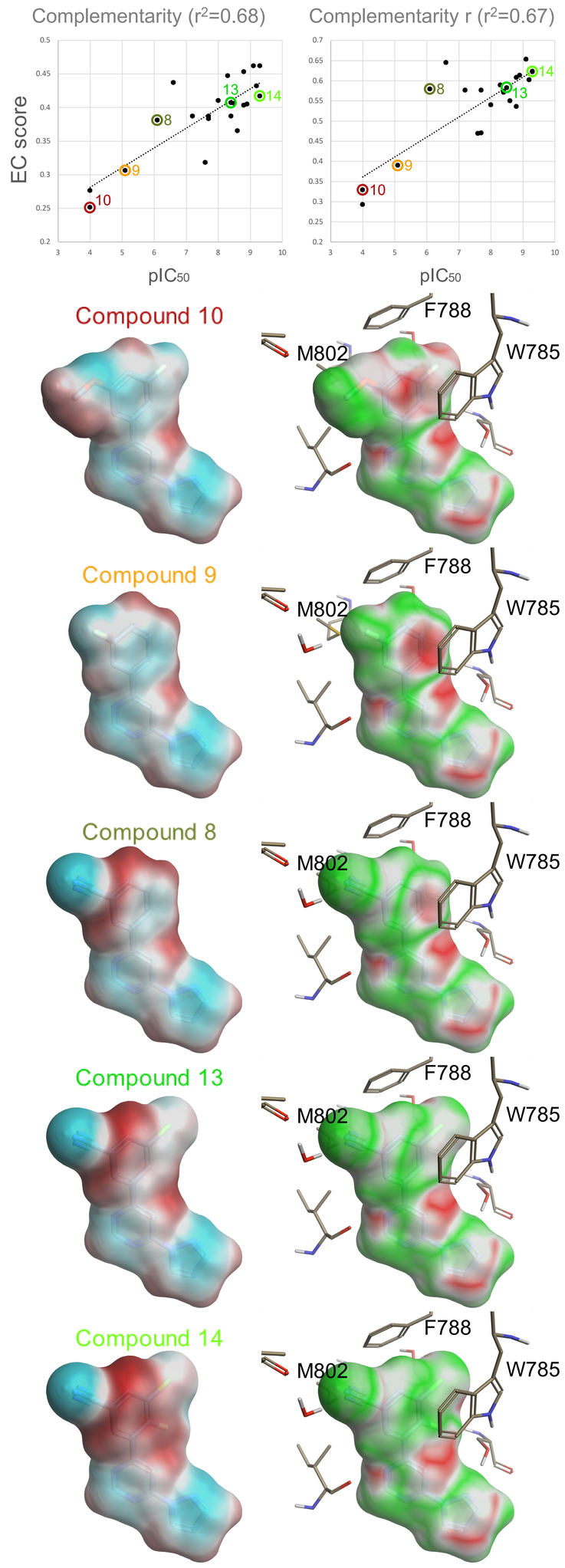

Figure 2: Comparison of ESP and EC surfaces of 5 representative mGLU5 ligands with increasing pIC_{50} values. With decreasing negative potential of the phenyl π-plane (left panel) via introduction of electron withdrawing groups, the electrostatic clash (right panel) between the phenyl ring and the aromatic indole of W785 side chain is minimized.

XIAP

Chessari *et al.* recently reported small molecule inhibitors of the XIAP / c-IAP-caspase protein-protein interaction.[5] A particularly interesting feature of this data set was the strong correlation of compound potency with Hammett σ_p values of substituents on the aromatic part of the indoline ring. This finding was rationalized with the electrostatic clash between the aromatic indoline system with a backbone carbonyl group and a phenolic tyrosine oxygen using DFT ESP calculations and Cresset field point technology.[4]

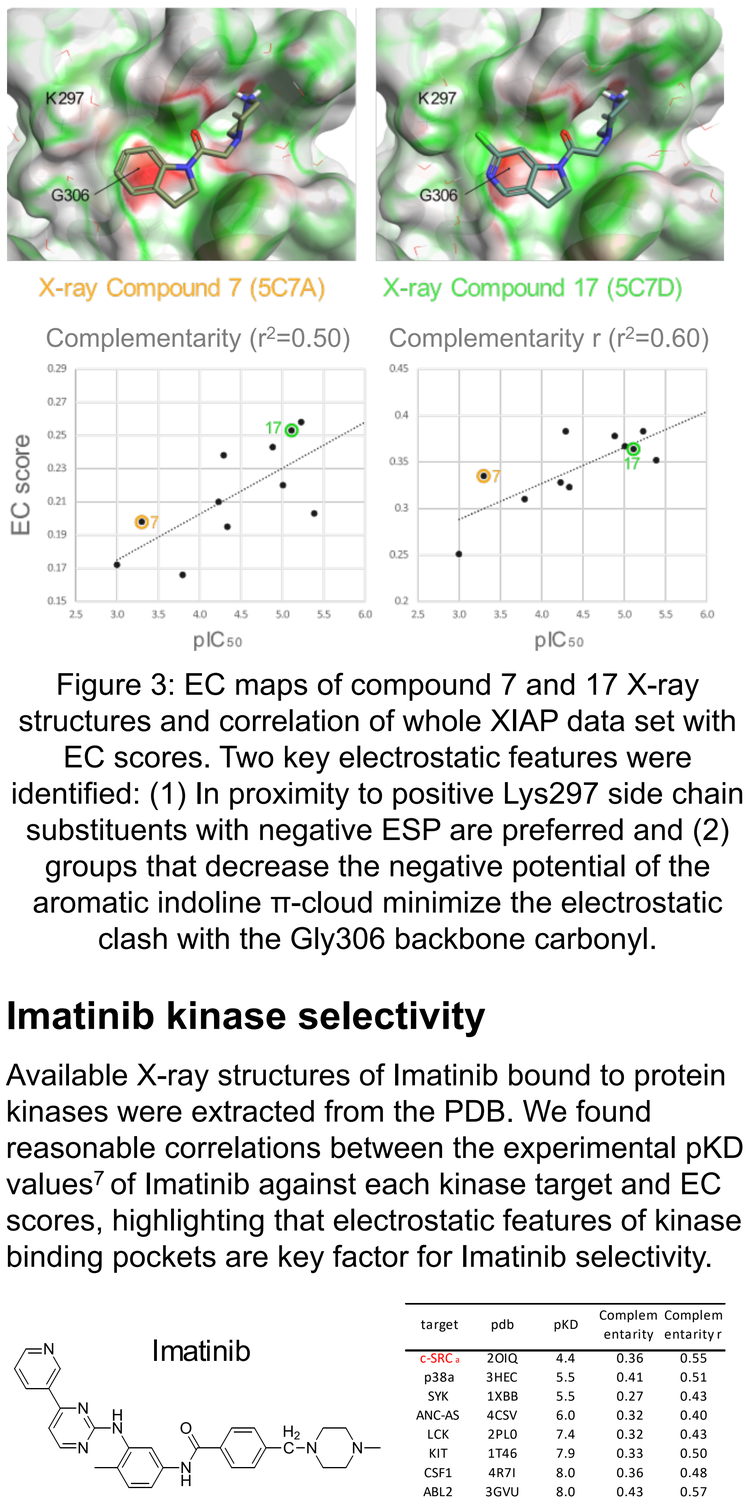

Figure 3: EC maps of compound 7 and 17 X-ray structures and correlation of whole XIAP data set with EC scores. Two key electrostatic features were identified: (1) In proximity to positive Lys297 side chain substituents with negative ESP are preferred and (2) groups that decrease the negative potential of the aromatic indoline π-cloud minimize the electrostatic clash with the Gly306 backbone carbonyl.

Imatinib kinase selectivity

Available X-ray structures of Imatinib bound to protein kinases were extracted from the PDB. We found reasonable correlations between the experimental pKD values[7] of Imatinib against each kinase target and EC scores, highlighting that electrostatic features of kinase binding pockets are key factor for Imatinib selectivity.

target	pdb	pKD	Complementarity	Complementarity r
c-SRC [a]	2OIQ	4.4	0.36	0.55
p38a	3HEC	5.5	0.41	0.51
SYK	1XBB	5.5	0.27	0.43
ANC-AS	4CSV	6.0	0.32	0.40
LCK	2PL0	7.4	0.32	0.43
KIT	1T46	7.9	0.33	0.50
CSF1	4R7I	8.0	0.36	0.48
ABL2	3GVU	8.0	0.43	0.57
ABL	1OPJ	9.0	0.43	0.63
DDR1	4BKJ	9.1	0.41	0.57

[a] Imatinib binding decreased due to conf penalty upon binding

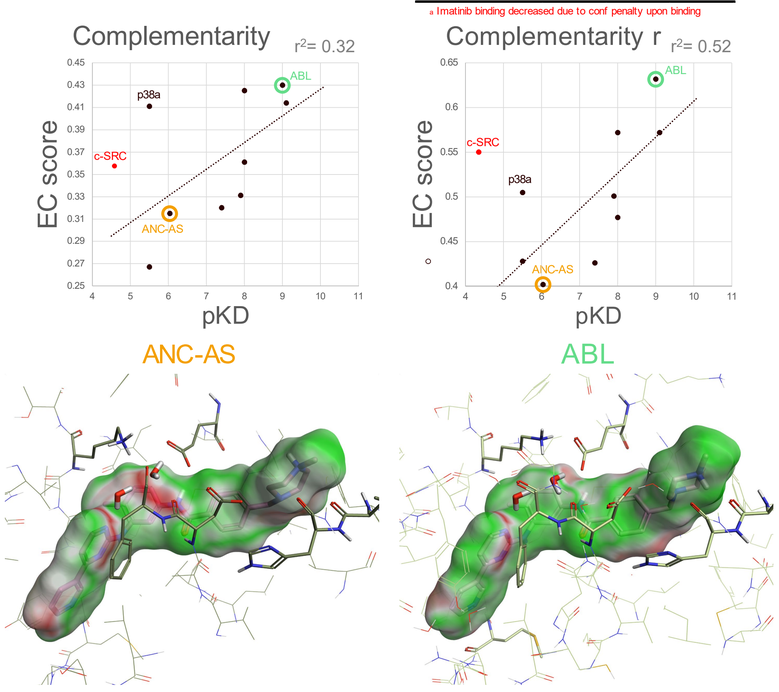

Figure 4: Predicting imatinib kinase selectivity. EC scores correlate with pKD values. EC maps highlight differences between imatinib binding to ABL and ANC-AS kinases.

Conclusion

Application of EC to reported mGLU5 and XIAP data sets showed that our method can detect and quantify electrostatic differences that cause changes in bioactivity. Furthermore, selectivity of Imatinib to a panel of kinases could be predicted via EC scoring. EC scores and maps in Flare, provide rapid activity prediction with visual feedback on new molecule designs. They provide useful information for understanding ligand binding and SAR and can be used for rapid ranking of new molecule designs.

References

1. https://cresset-group.com/flare
2. Vinter, J. G., Comput. Aided Mol. Des. 1994, 8 (6), 653–668
3. Vinter, J. G., Comput. Aided Mol. Des. 1996, 10 (5), 417–426
4. Cheeseright, T. *et al*., J. Chem. Inf. Model. 2006, 46 (2), 665–676.
5. Chessari, G. *et al*., J. Med. Chem. 2015, 58 (16), 6574-6588
6. Christopher, J. A. *et al*., J. Med. Chem. 2015, 58 (16), 6653–6664.
7. Davis, M. I. *et al*., Nat Biotechnol. 2011, 29 (11), 1046-51